

Computation of transient radiation in semi-infinite regions based on exact nonreflecting boundary conditions and mixed time integration

Lonny L. Thompson * and Runnong Huan

Department of Mechanical Engineering, Clemson University, Clemson, SC 29634, USA

Abstract

Transient radiation in a semi-infinite region, bounded by a planar infinite baffle with a local acoustic source is considered. The numerical simulation of the transient radiation problem requires an artificial boundary Γ , here chosen to be a hemisphere, which separates the computational region from the surrounding unbounded acoustic medium. Inside the computational region we use a semidiscrete finite element method. On Γ , we apply the exact nonreflecting boundary condition (NRBC) first derived by Grote and Keller for the free-space problem. Since the problem is symmetric about the infinite planar surface, in order to satisfy the rigid baffle condition it is sufficient to restrict the indices in the spherical harmonic expansion which defines the NRBC and scale the radial harmonics which drive auxiliary equations on the boundary. The Fourier expansion in the circumferential angle appearing in the NRBC may be used to efficiently model axisymmetric problems in two-dimensions. A new mixed explicit-implicit time integration method which retains the efficiency of explicit pressure field updates without the need for diagonal matrices in the auxiliary equations on Γ is presented. Here, the interior finite element equations are integrated explicitly in time while the auxiliary equations are integrated implicitly. The result is a very natural and highly efficient algorithm for large-scale wave propagation analysis. Numerical examples of fully transient radiation resulting from a piston transducer mounted in an infinite planar baffle are compared to analytical solutions to demonstrate the accuracy of the mixed time integration method with the NRBC for the half-space problem.

Journal of the Acoustical Society of America, Vol. 106, No. 6, pp. 3095-3108, Dec. 1999

*Corresponding Author.

1 Introduction

We consider the problem of determining the transient acoustic field radiated from an arbitrary shaped transducer or vibrating structure in a semi-infinite three-dimensional region, bounded by a planar infinite baffle. Modeling of local acoustic sources in a half-space has broad application including, numerical simulation of piezoelectric transduction systems; ultrasonics and non-destructive testing, and non-invasive therapeutic applications such as high intensity focused ultrasound. Examples include ring transducers used in sonar devices [1] and geometrically focused transducers [2]. Often, the transducer must deliver a precise acoustic near field radiation pattern which is difficult to measure experimentally [3]. For this reason, in recent years, there has been increased interest in the use of numerical simulation to predict the acoustic radiation field and to aid in the design of optimal transduction systems, e.g. [4, 5].

When modeling transient radiation/scattering from structures in an acoustic medium which extends to infinity with finite element/difference/volume methods, the computational domain must be truncated at a finite distance from the structure. The impedance of the unbounded domain exterior to the artificial truncation boundary is then represented on this boundary by either absorbing boundary conditions, infinite elements, or matched ‘sponge’ layers. Survey articles of various boundary treatments are given in [6]. If accurate boundary treatments are used, the finite computational region can be reduced so that the truncation boundary is relatively close to the radiator/scatterer, and fewer acoustic elements than otherwise would be possible may be used, resulting in considerable savings in both cpu time and memory. In the frequency domain, several accurate and efficient methods for representing the impedance of the far-field are well understood, including the Dirichlet-to-Neumann (DtN) map [7, 8], and infinite elements [9]. However, efficient evaluation of accurate boundary treatments for the time-dependent wave equation on unbounded spatial domains has long been an obstacle for the development of reliable solvers for time domain simulations. Ideally, the artificial boundary would be placed as close as possible to the source, and the radiation boundary treatment would be capable of arbitrary accuracy at a cost and memory not exceeding that of the interior solver.

A standard approach is to apply local (differential) boundary operators which annihilate leading terms in the radial multipole expansion for outgoing wave solutions. A well known sequence of boundary conditions developed for a spherical truncation boundary are the local operators derived by Bayliss and Turkel [10]. Because these operators involve only local spatial derivatives, while derived for a spherical boundary in free space, they may be used without alteration for semi-infinite regions, such as the problem of a transducer mounted in an infinite half-space. However, these and other approximate local boundary conditions exhibit significant spurious reflection for high-order wave harmonics, especially as the position of the truncation boundary approaches the source of radiation [11, 12]. In addition, as the order of these local non-reflecting boundary conditions increases they become increasingly difficult to implement in standard semidiscrete finite element formulations due to the occurrence of high-order time derivatives on the truncation boundary.

In recent years, new boundary treatments have been developed which dramatically improve both the accuracy and efficiency of time domain simulations compared to approximate local radiation boundary conditions. One promising approach is the

application of the ‘perfectly matched layer’ (PML) technique [14, 15] which introduces an external layer designed to absorb outgoing waves. In [16, 17], exact nonreflecting boundary conditions (NRBC) are derived for the free-space problem involving solution of an auxiliary Cauchy problem for linear first-order systems of time-dependent differential equations on a spherical boundary for each harmonic. In [18], the NRBC is rederived based on direct application of a result given in Lamb [22], with improved scaling of the first-order system of equations associated with the NRBC. This rescaling improves the numerical conditioning of the first-order system of equations when solved with implicit methods. Formulation of the NRBC in standard semidiscrete finite element methods with several alternative implicit and explicit time-integrators is reported in [18, 19]. When implemented in the finite element method, NRBC requires inner products of spherical harmonics and standard C^0 continuous basis functions with compact support, appearing in the force vector. As a result, the NRBC may be implemented efficiently and does not disturb the symmetric and banded/sparse structure of the finite element matrix equations. In [20], an efficient method is described for calculating far field solutions concurrently with the near-field solution based on the exact NRBC.

In [19], a modified version of the exact NRBC for the free-space problem with improved accuracy for high-order harmonics is formulated. To obtain a symmetric finite element variational equation, an additional auxiliary function is introduced on the artificial truncation boundary. This modified version may be viewed as an extension of the second-order local boundary operator derived by Bayliss and Turkel [10]. In [19] an implicit time discretization scheme is developed to integrate the semidiscrete finite element equations. However, in three-dimensions because of the difficulty in obtaining diagonal matrices for the auxiliary equations, a fully explicit time discretization which uncouples the system of equations was not possible.

Motivated by the excellent accuracy of the NRBC for the free-space problem, it is natural to extend these ideas to the problem of radiation in a semi-infinite acoustic domain resulting from transducers or vibrating structures mounted in a half-plane. However, as a result of the nonlocal spherical transform and expansion on a spherical boundary in free space, the NRBC must be modified for the infinite half-space problem. In this work, we give the extension of the exact NRBC originally derived by Grote and Keller [16] for the free-space problem for application to semi-infinite problems defined by an infinite planar baffle. Two alternative forms of the NRBC which satisfy the symmetry condition imposed by the rigid baffle are possible; in the first we orient the baffle normal (perpendicular) to a z -axis of revolution defined in spherical coordinates; while in the second the baffle is aligned (parallel) with the z -axis. The advantage of the first approach is that axisymmetric radiation in a half-space may be modeled efficiently in two-dimensions.

For the symmetric form of the modified NRBC we give a new mixed explicit-implicit time integration method which retains the efficiency of explicit time discretization for the finite element matrix equations, without the need for diagonal matrices in the auxiliary equations on the artificial truncation boundary. Here, the interior finite element equations are integrated explicitly in time while the auxiliary equations are integrated implicitly in time. By treating the auxiliary equations on the boundary implicitly, a very natural and highly efficient algorithm is developed for large-scale wave propagation analysis which allows the pressure field to be updated

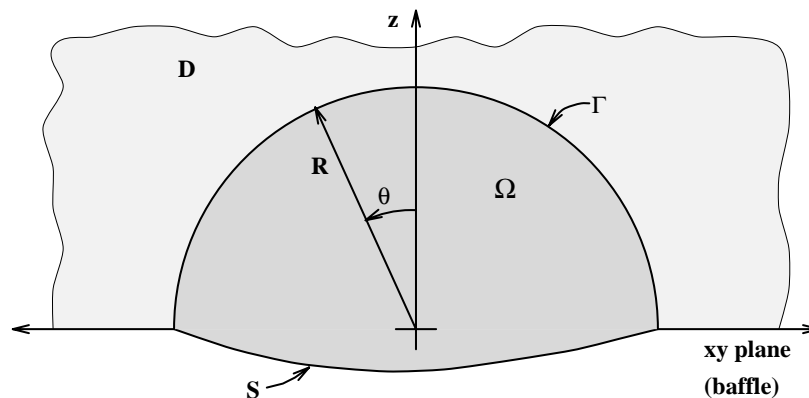


Fig. 1: Illustration of semi-infinite region lying on one side of a boundary composed of an arbitrary radiation surface \mathcal{S} and the xy plane. The computational domain Ω is surrounded by a semi-spherical truncation boundary Γ . Exterior region denoted by \mathcal{D} .

without assembling or factoring the interior finite element matrices.

In [18, 19] numerical experiments for radiation from a sphere in free-space are presented which demonstrate the accuracy of the NRBC compared to steady-state analytical solutions and standard local absorbing boundary conditions. In this work, numerical results for fully transient solutions for a circular transducer mounted in an infinite rigid planar baffle are compared to analytical solutions. The numerical results are used to assess the accuracy of the mixed explicit-implicit time integration method with the NRBC restricted for the half-space problem.

2 Transient Radiation In Acoustic Half-space

We consider time-dependent scattering/radiation in a three-dimensional semi-infinite region bounded by a boundary composed of an arbitrary shaped radiation surface \mathcal{S} and a planar infinite baffle (see Fig. 1). We denote the space above this plane as the semi-infinite region \mathcal{R} . The numerical simulation of the transient radiation problem requires an artificial boundary Γ , here chosen to be a semi-sphere of radius $\|\mathbf{x}\| = R$, which separates the computational region Ω from the surrounded unbounded acoustic medium. At R we impose an absorbing boundary condition to reduce spurious reflection from it. Inhomogeneities and nonlinear sources may be incorporated within the computational domain while the remainder of the problem is treated as a homogeneous acoustic medium occupying an infinite half-space and is dealt with through the domain truncation boundary.

Within Ω the acoustic pressure $p(\mathbf{x}, t)$ satisfies the scalar wave equation:

$$\nabla^2 p - \frac{1}{c^2} \frac{\partial^2 p}{\partial t^2} = -f, \quad \mathbf{x} \text{ in } \Omega, t > 0 \quad (1)$$

with initial conditions,

$$p(\mathbf{x}, 0) = p_0(\mathbf{x}), \quad \frac{\partial p}{\partial t}(\mathbf{x}, 0) = \dot{p}_0(\mathbf{x}), \quad \mathbf{x} \in \Omega \quad (2)$$

and driven by a normal velocity $v = -\mathbf{v} \cdot \mathbf{n}$, prescribed on the radiation boundary \mathcal{S} :

$$\frac{\partial p}{\partial n} = \rho_o \dot{v}(\mathbf{x}, t), \quad \mathbf{x} \in \mathcal{S}, t > 0 \quad (3)$$

In the above, $c(\mathbf{x})$ is the velocity of sound in the acoustic medium, $\rho_o(\mathbf{x})$ is the mass density, a superimposed dot denotes a time-derivative, and \mathbf{n} is an outward pointing normal vector. The normal velocity represents the time-dependent motion of the transducer. The normal velocity $v(\mathbf{x}, t)$, acoustic source $f(\mathbf{x}, t)$, and initial data are assumed to be confined to the interior of the region Ω , so that in the infinite half-space, i.e., the region outside Γ , the acoustic pressure field $p(\mathbf{x}, t)$ satisfies the homogeneous form of the wave equation with constant wave speed c ,

$$\nabla^2 p - \frac{1}{c^2} \frac{\partial^2 p}{\partial t^2} = 0 \quad \mathbf{x} \text{ in } \mathcal{D}, t > 0 \quad (4)$$

$$p(\mathbf{x}, 0) = 0, \quad \frac{\partial p}{\partial t}(\mathbf{x}, 0) = 0, \quad \mathbf{x} \in \mathcal{D} \quad (5)$$

and the homogeneous Neumann boundary condition imposed by the rigid baffle,

$$\frac{\partial p}{\partial n} = 0, \quad \mathbf{x} \in \mathcal{S}, t > 0 \quad (6)$$

In the following, we introduce spherical coordinates (r, θ, φ) ,

$$x = r \cos \varphi \sin \theta \quad (7)$$

$$y = r \sin \varphi \sin \theta \quad (8)$$

$$z = r \cos \theta \quad (9)$$

such that the z -axis is aligned *perpendicular* (normal) to the planar baffle.

With this parameterization, the artificial boundary is defined by the hemisphere,

$$\Gamma := \{r = R, 0 < \theta \leq \pi/2, 0 < \varphi \leq 2\pi\}$$

and a general solution to the wave equation (4) in the exterior region $\mathcal{D} = \{r \geq R, 0 \leq \theta \leq \pi/2, 0 \leq \varphi < 2\pi\}$ may expanded as,

$$p(r, \theta, \varphi, t) = \sum_{n=0}^{\infty} \sum_{m=0}^n {}' P_n^m(\cos \theta) (p_{nm}^c(r, t) \cos m\varphi + p_{nm}^s(r, t) \sin m\varphi) \quad (10)$$

Here P_n^m is the associated Legendre function of the first kind, and the prime on the sum indicates that a factor of 1/2 multiplies the term with $m = 0$. The radial harmonics associated with the even and odd trigonometric functions are computed from,

$$p_{nm}^c = \frac{2}{N_{nm}} \int_0^{2\pi} \int_0^{\pi/2} p(r, \theta, \varphi, t) P_n^m(\cos \theta) \cos m\varphi \sin \theta d\theta d\varphi \quad (11)$$

$$p_{nm}^s = \frac{2}{N_{nm}} \int_0^{2\pi} \int_0^{\pi/2} p(r, \theta, \varphi, t) P_n^m(\cos \theta) \sin m\varphi \sin \theta d\theta d\varphi \quad (12)$$

where N_{nm} is the normalization factor for the orthogonal spherical harmonics;

$$N_{nm} = \frac{2\pi(n+m)!}{(2n+1)(n-m)!} \quad (13)$$

For the semi-infinite region defined by the half-space \mathcal{D} , the multiplier 2 appearing in (11) and (12) results from integration restricted over the hemisphere only; the limits of integration ranging from $0 \leq \theta \leq \pi/2$.

Since the problem is symmetric about the rigid planar baffle at $\theta = \pi/2$, i.e.,

$$\left. \frac{\partial p}{\partial \theta} \right|_{\theta=\pi/2} = -r \left. \frac{\partial p}{\partial z} \right|_{z=0} = 0, \quad r \geq R \quad (14)$$

it is sufficient to restrict the expansion (10) in spherical harmonics to indices $n+m$ even. While this modification is trivial, it is not necessarily obvious. To prove this result, we evaluate the expansion (10) at $\theta = \pi/2$,

$$\left. \frac{\partial p}{\partial \theta} \right|_{\theta=\pi/2} = \sum_{n=0}^{\infty} \sum_{m=0}^n P_n^m(0) (p_{nm}^c(r, t) \cos m\varphi + p_{nm}^s(r, t) \sin m\varphi) \quad (15)$$

From properties of the associated Legendre functions [21],

$$P_n^m(0) = \begin{cases} 0 & n+m = \text{even} \\ (-1)^{(m+n-1)/2} \frac{1 \cdot 3 \cdot 5 \cdots (n+m)}{2 \cdot 4 \cdot 6 \cdots (n-m-1)} & n+m = \text{odd.} \end{cases} \quad (16)$$

only the combination $n+m = \text{even}$, satisfies $P_n^m(0) = 0$, and it follows that expansion (10) satisfies (15) only with the restriction $n+m = \text{even}$.

3 Exact NRBC's On A Hemisphere

On the artificial boundary Γ the radial functions p_{nm}^c and p_{nm}^s appearing in (10) satisfy the boundary condition derived in [16, 18] for a spherical boundary in free-space:

$$B_1[p_{nm}] = -\frac{1}{r} \mathbf{c}_n \cdot \mathbf{z}_{nm}(t), \quad r = R \quad (17)$$

where

$$B_1[p_{nm}] := \left(\frac{\partial}{\partial r} + \frac{1}{c} \frac{\partial}{\partial t} + \frac{1}{r} \right) p_{nm} \quad (18)$$

is the 'first-order' local boundary operator of Bayliss and Turkel [10]. The constant n -component vector $\mathbf{c}_n = \{c_n^j\}$ is defined with coefficients,

$$c_n^j = n(n+1)j/2R, \quad j = 1, 2, \dots, n \quad (19)$$

while the vector functions $\mathbf{z}_{nm}(t) = \{z_{nm}^j(t)\}$, $j = 1, \dots, n$ of order n satisfy the first-order system of ordinary differential equations,

$$\begin{aligned} \frac{d}{dt} \mathbf{z}_{nm}(t) &= \mathbf{A}_n \mathbf{z}_{nm}(t) + c \Phi_{nm}(t) \\ \mathbf{z}_{nm}(0) &= 0 \end{aligned} \quad (20)$$

with constant $n \times n$ matrices $\mathbf{A}_n = \{A_n^{ij}\}$ defined with coefficients [18]:

$$A_n^{ij} = \begin{cases} \frac{-n(n+1)c}{2R} & \text{if } i = 1 \\ \frac{(n+i)(n-i+1)c}{2iR} & \text{if } i = j + 1 \\ 0 & \text{otherwise} \end{cases} \quad (21)$$

For the semi-infinite half-space problem considered here, the system (20) is driven by the time-dependent vector function,

$$\Phi_{nm}(t) = [c p_{nm}|_{r=R}, 0, \dots, 0]^T. \quad (22)$$

with radial modes evaluated at $r = R$, $p_{nm}|_{r=R}$, computed from (11) and (12).

The exact nonreflecting boundary condition (NRBC) for the half-space problem on the hemisphere Γ is obtained by multiplying (17) by spherical harmonics, summing over n and m , setting $r = R$ and using (10),

$$B_1[p] = -\frac{1}{R} \sum_{n=1}^{\infty} \sum_{m=0}^n P_n^m(\cos \theta) (w_{nm}^c(t) \cos m\varphi + w_{nm}^s(t) \sin m\varphi), \quad n+m = \text{even} \quad (23)$$

where $w_{nm}^c = \mathbf{c}_{nm} \cdot \mathbf{z}_{nm}^c$ and $w_{nm}^s = \mathbf{c}_{nm} \cdot \mathbf{z}_{nm}^s$ are scalar functions defined by the even and odd harmonics in φ . This condition is the same as the free-space problem derived in [16, 18], except that for the rigid baffle symmetry condition, the indices are restricted to $n + m = \text{even}$, and the radial harmonics include a factor of 2 resulting from integration over a hemisphere.

Alternatively, the z -axis may be *aligned* (parallel) with the infinite baffle such that the hemisphere is defined by, $\Gamma := \{r = R, 0 < \theta \leq \pi, 0 < \phi \leq \pi\}$. With this orientation, the symmetry condition imposed by the rigid planar baffle is satisfied by restricting the Fourier expansion in (10) to even functions $\cos m\phi$. In this case, the exact nonreflecting boundary condition for the hemisphere may be written as,

$$B_1[p] = -\frac{1}{R} \sum_{n=1}^{\infty} \sum_{m=0}^n \mathbf{c}_n \cdot \mathbf{z}_{nm}(t) P_n^m(\cos \theta) \cos m\phi \quad \text{on } \Gamma \quad (24)$$

where the system of equations (20) for \mathbf{z}_{nm} is driven by the radial modes,

$$p_{nm}|_{r=R} = \frac{2}{N_{nm}} \int_0^\pi \int_0^\pi p(R, \theta, \phi, t) P_n^m(\cos \theta) \cos m\phi \sin \theta d\theta d\phi \quad (25)$$

with integration restricted over the range $0 \leq \phi \leq \pi$.

4 Axisymmetric Problems

For general problems in three-dimensions, the two forms of the NRBC (23) and (24) have the same storage requirements and operation counts. An advantage in expressing the NRBC in the form (23) is that axisymmetric problems in a half-space defined by a planar baffle may be solved efficiently with a periodic Fourier expansion in φ and imposing the planar symmetry condition in the Legendre function expansion in θ . In this case an efficient solution is obtained by reducing the axisymmetric problem to a sequence of uncoupled two-dimensional problems with a Fourier expansion in the circumferential direction φ about a z -axis of revolution perpendicular to the planar baffle. This reduction is not possible with the NRBC expressed in the form (24) since the Fourier harmonics are restricted by the baffle condition. An example of axisymmetric radiation in a half-space is given by the classic model of transient radiation from a circular piston mounted in an infinite planar baffle (see numerical examples in Section 5).

To be specific, for radiation surfaces \mathcal{S} with axisymmetric geometry about a z -axis *perpendicular* (normal) to the planar baffle, and driven by acoustic sources (3) which are periodic in the angle of revolution φ , i.e.,

$$\dot{v}(\mathbf{x}, t) = \sum_{m=0}^{\infty} ' [g_m^c(r, \theta, t) \cos m\varphi + g_m^s(r, \theta, t) \sin m\varphi] \quad (26)$$

then the pressure may be expressed by the Fourier series,

$$p = \sum_{m=0}^{\infty} ' [p_m^c(r, \theta, t) \cos m\varphi + p_m^s(r, \theta, t) \sin m\varphi] \quad (27)$$

In this case, the pressure field decouples for different Fourier harmonics m due to the orthogonality of the trigonometric functions and the problem simplifies to solving for the Fourier modes $p_m^c(r, \theta, t)$ and $p_m^s(r, \theta, t)$ in a two-dimensional half-plane defined by the cylindrical coordinates (ρ, z) , with $\rho = r \sin \theta$ and $z = r \cos \theta$. Outgoing solutions for the modes p_m are absorbed exactly by imposing the NRBC in the form (23) with the variation in φ suppressed, i.e.,

$$B_1[p_m] = -\frac{1}{R} \sum_{n=1}^{\infty} \mathbf{c}_n \cdot \mathbf{z}_{nm}(t) P_n^m(\cos \theta), \quad n + m = \text{even} \quad (28)$$

In the above $\mathbf{c}_n \cdot \mathbf{z}_{nm}(t) = w_{nm}^c(t)$ for modes $p_m = p_m^c$, and $\mathbf{c}_n \cdot \mathbf{z}_{nm}(t) = w_{nm}^s(t)$ for modes $p_m = p_m^s$. For the rigid baffle condition, the indices in the Legendre function expansion remain restricted to $n + m$ even, and the system of equations (20) for \mathbf{z}_{nm} are driven by radial modes p_{nm} computed from the restricted Legendre transform,

$$p_{nm}|_{r=R} = \frac{2\pi}{N_{nm}} \int_0^{\pi/2} p_m(r, \theta, t) P_n^m(\cos \theta) \sin \theta d\theta \quad (29)$$

When driven by sources $\dot{v} = g_0$ which are independent of the angle of revolution φ , the pressure field is defined by the single mode $p = p_0(r, \theta, t)$, and the exact NRBC

reduces naturally by setting the index $m = 0$ in (23), with the result,

$$B_1[p] = -\frac{1}{R} \sum_{n=2,4,\dots}^{\infty} \mathbf{c}_n \cdot \mathbf{z}_{n0}(t) P_n(\cos \theta) \quad (30)$$

Here the system of equations (20) for \mathbf{z}_{n0} are driven by the radial modes,

$$p_{n0}|_{r=R} = (2n + 1) \int_0^{\pi/2} p(R, \theta, t) P_n(\cos \theta) \sin \theta d\theta \quad (31)$$

with integration restricted over the quarter circle, $0 \leq \theta < \pi/2$.

5 Modified NRBC's on a Hemisphere

In practice, the infinite sum over n in (23) or (24) is truncated at a finite value N . In this case, we denote the boundary condition by NR1(N), where N defines the number of harmonics included in the truncated series. Use of NR1(N) on a hemisphere with boundary Γ will exactly represent all harmonics $p_{nm}(r, t)$, for $n \leq N$ in the outgoing solution to the initial-boundary value problem for the half-space. For $n > N$, then NR1(N) approximates the harmonics with the local operator $B_1[p] = 0$ on Γ , with leading error of order, $B_1[p] = O(\frac{1}{R^3})$. Accuracy of the approximated harmonics $n > N$, may be improved by increasing the radius of the truncation boundary R , but at the added expense of a larger computation region Ω , resulting in increased memory and cpu times.

To improve the approximation to the truncated harmonics $n > N$, without affecting the modes $n \leq N$, the second-order local boundary operator,

$$B_2[p_{nm}] := \left(\frac{\partial}{\partial r} + \frac{1}{c} \frac{\partial}{\partial t} + \frac{3}{r} \right) B_1[p_{nm}] \quad (32)$$

of Bayliss and Turkel [10] may be used to obtain a modified boundary condition for the radial modes [17, 19]:

$$B_2[p_{nm}] = \frac{1}{r} \tilde{\mathbf{c}}_n \cdot \mathbf{z}_{nm}(t), \quad r = R \quad (33)$$

Here the coefficient vector $\tilde{\mathbf{c}}_n = \{\tilde{c}_n^j\}$ is given by,

$$\tilde{c}_n^j = n(n+1)j(j-1)/2R^2, \quad j = 1, 2, \dots, n \quad (34)$$

and the vector functions $\mathbf{z}_{nm}(t)$ appearing in (33) satisfy the same first-order system of ordinary differential equations (20), driven by (22). This modified condition was first derived in [17] for a spherical boundary Γ in free-space and modified in [19] with improved scaling $\tilde{\mathbf{c}}_{nm}$.

To obtain an equivalent but more tractable form for finite element implementation, the second-order radial derivative appearing in the local B_2 operator defined in (32), is eliminated using the radial wave equation for the modes p_{nm} ,

$$\frac{\partial^2 p_{nm}}{\partial r^2} = \frac{1}{c^2} \frac{\partial^2 p_{nm}}{\partial t^2} - \frac{2}{r} \frac{\partial p_{nm}}{\partial r} + \frac{n(n+1)}{r^2} p_{nm}. \quad (35)$$

with the result,

$$\frac{r}{c} \frac{\partial}{\partial t} B_1[p_{nm}] + B_1[p_{nm}] + \frac{n(n+1)}{2r} p_{nm} = \frac{1}{2} \tilde{\mathbf{c}}_n \cdot \mathbf{z}_{nm}(t), \quad r = R \quad (36)$$

With the z -axis oriented perpendicular (normal) to the infinite planar baffle, then multiplying (36) by the spherical harmonics defined in (10), gives the modified NRBC:

$$\hat{B}_2[p] = \frac{1}{2} \sum_{n=2}^N \sum_{m=0}^n ' P_n^m(\cos \theta) (\tilde{w}_{nm}^c(t) \cos m\varphi + \tilde{w}_{nm}^s(t) \sin m\varphi), \quad n+m = \text{even} \quad (37)$$

$$\hat{B}_2[p] := \frac{R}{c} \frac{\partial}{\partial t} B_1[p] + B_1[p] - \frac{1}{2R} \Delta_\Gamma[p] \quad (38)$$

$$\Delta_\Gamma[p] := \frac{1}{\sin \theta} \frac{\partial}{\partial \theta} \left(\sin \theta \frac{\partial p}{\partial \theta} \right) + \frac{1}{\sin^2 \theta} \frac{\partial^2 p}{\partial \varphi^2} \quad (39)$$

where $\tilde{w}_{nm} = \tilde{\mathbf{c}}_n \cdot \mathbf{z}_{nm}(t)$. This modified condition takes the same form as the free-space problem derived in [19]. Here, the indices are restricted to $n+m = \text{even}$ in order to satisfy the rigid baffle condition.

We denote (37) by NR2(N). Use of NR2(N) will exactly represent all harmonics $p_{nm}(r, t)$, for $n \leq N$ on a semi-spherical truncation boundary for the half-plane. For $n > N$, the truncated condition (37) reduces to $B_2[p] = 0$ on Γ . This condition approximates the harmonics $n > N$, with leading error of the order, $B_2[p] = \mathcal{O}(\frac{1}{R^5})$. Therefore, when truncated at a finite value N , the modified condition approximates the truncated harmonics $n > N$ with greater accuracy than NR1.

In [19], we show how a modified boundary condition in the form (37) can be implemented in a symmetric finite element variational formulation for the free-space problem by introducing additional auxiliary functions $q_{nm}(t)$ and $\psi(\theta, \varphi, t)$, such that:

$$B_1[p] - \frac{1}{2R} \Delta_\Gamma[\psi] = \frac{1}{2} \sum_{n=2}^N \sum_{m=0}^n ' P_n^m(\cos \theta) (q_{nm}^c(t) \cos m\varphi + q_{nm}^s(t) \sin m\varphi) \quad (40)$$

$$\left(\frac{R}{c} \frac{\partial}{\partial t} + 1 \right) \Delta_\Gamma[\psi] = \Delta_\Gamma[p], \quad \psi(\theta, \varphi, 0) = 0 \quad (41)$$

and q_{nm}^c and q_{nm}^s satisfy,

$$\left(\frac{R}{c} \frac{d}{dt} + 1 \right) q_{nm}(t) = \tilde{\mathbf{c}}_n \cdot \mathbf{z}_{nm}(t), \quad q_{nm}(0) = 0 \quad (42)$$

The three equations (40), (41), and (42), define an equivalent form of the exact NRBC (37), suitable for implementation in a symmetric finite element formulation. With the z -axis oriented perpendicular (normal) to the planar rigid baffle, it is sufficient to restrict the expansion in spherical harmonics given in (40) to indices $n + m$ even.

Alternatively, with the z -axis aligned (parallel) with the planar baffle, the rigid condition is satisfied with the expansion,

$$B_1[p] - \frac{1}{2R}\Delta_\Gamma[\psi] = \frac{1}{2} \sum_{n=2}^N \sum_{m=0}^n q_{nm}(t) P_n(\cos\theta) \cos m\phi \quad (43)$$

Again, the advantage of the form (40), based on a Fourier expansion in φ about a z -axis of revolution oriented normal to the planar baffle, is that axisymmetric problems in a half-space can be modeled efficiently in two-dimensions.

6 Finite Element Formulation

Finite element discretization of the bounded acoustic region Ω , allows for a natural coupling to an elastic radiator on the surface \mathcal{S} . The finite element formulation of the NR1(N) defined in (23) or (24), and the symmetric form of NR2(N) defined in (40) or (43) for the half-space problem posed on a rigid planar baffle, follows the same form as given in [18, 19] for the free-space problem. By introducing finite element approximations, a system of ordinary differential equations are obtained which must then be integrated in time. In the following, we summarize the semidiscrete matrix equations resulting from the symmetric form of NR2(N) and then present a new mixed explicit/implicit time-integration method for advancing the solution.

6.1 Finite Element Discretization

The finite element discretization is obtained by approximating the variational equation associated with the wave equation and the nonreflecting boundary condition. The variational equation within Ω is obtained by multiplying (1) with a weighting function δp and using the divergence theorem. For the symmetric NR2(N) condition, an auxiliary equation on Γ is obtained by multiplying (41) with a different weighting function $\delta\psi$, then integrating by parts. Using independent finite element approximations,

$$p(\mathbf{x}, t) \approx \mathbf{N}_p(\mathbf{x})\mathbf{p}(t) \text{ in } \Omega \cup \partial\Omega \quad (44)$$

$$\psi(\mathbf{x}, t) \approx \mathbf{N}_\psi(\mathbf{x})\boldsymbol{\psi}(t) \text{ on } \Gamma \quad (45)$$

where \mathbf{N}_p and \mathbf{N}_ψ are standard vector arrays of C^0 basis functions with compact support associated with each node of the finite element mesh in $\Omega \cup \partial\Omega$, and on the boundary Γ , results in the following coupled, symmetric system of semidiscrete matrix equations,

$$\mathbf{M}_p \frac{d^2\mathbf{p}(t)}{dt^2} + \mathbf{C}_p \frac{d\mathbf{p}(t)}{dt} + \mathbf{K}_p\mathbf{p}(t) = \mathbf{F}(t) - \mathbf{A}\boldsymbol{\psi}(t), \quad (46)$$

$$\mathbf{C}_\psi \frac{d\boldsymbol{\psi}(t)}{dt} + \mathbf{K}_\psi \boldsymbol{\psi}(t) = \mathbf{A}^T \mathbf{p}(t), \quad (47)$$

The time-dependent vector $\mathbf{p}(t)$ determines the global solution at each node in the mesh, while $\boldsymbol{\psi}(t)$ is a vector of auxiliary parameters associated with the nodes on the truncation boundary. The symmetric arrays associated with the pressure field take the same form as the free-space problem given in [19],

$$\mathbf{M}_p = \int_{\Omega} \frac{1}{c^2} \mathbf{N}_p^T \mathbf{N}_p d\Omega \quad (48)$$

$$\mathbf{C}_p = \int_{\Gamma} \frac{1}{c} \mathbf{N}_p^T \mathbf{N}_p d\Gamma \quad (49)$$

$$\mathbf{K}_p = \int_{\Omega} (\nabla \mathbf{N}_p)^T (\nabla \mathbf{N}_p) d\Omega + \frac{1}{R} \int_{\Gamma} \mathbf{N}_p^T \mathbf{N}_p d\Gamma, \quad (50)$$

Similarly, the symmetric arrays associated with the auxiliary function ψ take the form,

$$\mathbf{C}_\psi = \frac{R^2}{2} \int_{\Gamma} \frac{1}{c} (\nabla^s \mathbf{N}_\psi)^T (\nabla^s \mathbf{N}_\psi) d\Gamma \quad (51)$$

$$\mathbf{K}_\psi = \frac{R}{2} \int_{\Gamma} (\nabla^s \mathbf{N}_\psi)^T (\nabla^s \mathbf{N}_\psi) d\Gamma \quad (52)$$

The coupling array between p and ψ is given by,

$$\mathbf{A} = \frac{R}{2} \int_{\Gamma} (\nabla^s \mathbf{N}_p)^T (\nabla^s \mathbf{N}_\psi) d\Gamma \quad (53)$$

where ∇^s denotes the surface gradient on a sphere and $d\Gamma = R^2 \sin \theta d\theta d\varphi$.

In deriving the matrix equations, second-order tangential derivatives appearing in Δ_{Γ} were reduced to first-order derivatives using integration-by-parts on the hemisphere Γ , i.e.,

$$\int_{\Gamma} \delta p \Delta_{\Gamma} \psi d\Gamma = -R^2 \int_{\Gamma} \nabla^s \delta p \cdot \nabla^s \psi d\Gamma \quad (54)$$

For the z -axis normal to the planar baffle, the above result follows from the symmetry condition in the angle θ , i.e., $\partial\psi/\partial\theta = 0$ at $\theta = \pi/2$, and the periodic condition in φ , i.e., $\delta p(R, \theta, 0) = \delta p(R, \theta, 2\pi)$.

The auxiliary functions ψ only appear as a surface gradient $\nabla^s \psi$. As a result, a family of solutions for ψ that differ by a constant will satisfy (47). To obtain a unique solution, the function ψ may be constrained at one arbitrary node on the truncation boundary. The value used to constrain the auxiliary function ψ at that node is inconsequential to the unique solution for p , and may be set to zero [19].

The semidiscrete equations are driven by the initial conditions and discrete force vector, $\mathbf{F}(t) = \mathbf{F}_S + \mathbf{F}_{\Gamma}$ composed of a standard load vector,

$$\mathbf{F}_S(t) = \int_{\Omega} \mathbf{N}_p^T f(\mathbf{x}, t) d\Omega + \int_S \mathbf{N}_p^T \rho_o \dot{v}(\mathbf{x}, t) dS \quad (55)$$

and a part associated with the auxiliary functions appearing in the NRBC,

$$\mathbf{F}_\Gamma(t) = \frac{1}{2} \sum_{n=2}^N \sum_{m=0}^n (q_{nm}^c(t) \mathbf{f}_{nm}^c + q_{nm}^s(t) \mathbf{f}_{nm}^s) \quad (56)$$

where,

$$\mathbf{f}_{nm}^c := \int_\Gamma \mathbf{N}_p^T P_n^m(\cos \theta) \cos m\varphi d\Gamma \quad (57)$$

$$\mathbf{f}_{nm}^s := \int_\Gamma \mathbf{N}_p^T P_n^m(\cos \theta) \sin m\varphi d\Gamma \quad (58)$$

With the z -axis normal to the rigid planar baffle, the indices appearing in (56) are restricted to $n + m = \text{even}$. The functions $q_{nm}(t)$ are solutions to the first-order equation (42), driven by the auxiliary variables $\mathbf{z}_{nm}(t)$. The vector functions \mathbf{z}_{nm} in turn, satisfy (20) driven by the radial modes on the hemisphere:

$$p_{nm}^c(R, t) = \frac{2}{R^2 N_{nm}} \mathbf{f}_{nm}^{cT} \cdot \mathbf{p}_\Gamma(t) \quad (59)$$

$$p_{nm}^s(R, t) = \frac{2}{R^2 N_{nm}} \mathbf{f}_{nm}^{sT} \cdot \mathbf{p}_\Gamma(t) \quad (60)$$

where $\mathbf{p}_\Gamma(t) = \{p_I(t)\}$, $I = 1, 2, \dots, N_\Gamma$, is a vector of nodal solutions on the artificial boundary Γ with N_Γ nodes.

Implementation of the non-reflecting boundary condition only requires inner products of spherical harmonics and finite element basis functions with compact support within the force vector \mathbf{f}_{nm} . As a result, the non-reflecting boundary condition is easy to implement using standard force vector assembly over each boundary element on Γ , and does not disturb the symmetric, and banded/sparse structure of the finite element matrix equations.

For axisymmetric radiation from a rigid baffle, the force vector (56) naturally specializes with the index restricted to $m = 0$, i.e.,

$$\mathbf{F}_\Gamma(t) = \pi R^2 \sum_{n=2,4,\dots}^N q_{n0}(t) \int_0^{\pi/2} \mathbf{N}_p^T P_n(\cos \theta) \sin \theta d\theta \quad (61)$$

where the system of equations (20) for \mathbf{z}_{n0} is driven by the radial modes given in (31).

7 Mixed Time Integration Algorithm

Both implicit and explicit time marching schemes have been developed in [18] to integrate the semi-discrete equations associated with the NR1(N) form of the exact nonreflecting condition on a spherical boundary in free-space. These time-integration algorithms may be used to implement the boundary condition (23) or (24) for the half

space problem with no significant modifications. For NR2(N), *implicit* time marching procedures developed in [19] may be applied directly to the coupled system of equations (46) and (47). However, direct application of *explicit* time stepping schemes which uncouple the system of equations is not possible due to the difficulty in generating an accurate diagonal matrix \mathbf{C}_ψ appearing in the auxiliary equations (47). Fully explicit time discretization with diagonal matrices drastically reduces computational cost and memory requirements. To obtain the efficiency of explicit time discretization without the need for a diagonal matrix \mathbf{C}_ψ , we present a new mixed explicit-implicit time integration method for solving the coupled system. Here, the interior finite element equations (46) are integrated explicitly in time and the auxiliary equations (47) on Γ are integrated implicitly in time. By treating the auxiliary equations implicitly, a very natural algorithm results which avoids the need to update either the pressure solutions or the auxiliary functions at intermediate time steps.

Let $\mathbf{F}^k = \mathbf{F}(t_k)$ be the force at time step $t_k = k \Delta t$. To compute the solution $\mathbf{p}^{k+1} = \mathbf{p}(t_{k+1})$, we apply the second-order accurate, *explicit* central difference method to the interior finite element matrix equations given in (46), with the result:

$$\hat{\mathbf{M}}\mathbf{p}^{k+1} = \mathbf{R}^k \quad (62)$$

with effective mass matrix,

$$\hat{\mathbf{M}} = \frac{1}{\Delta t^2}\mathbf{M}_p + \frac{1}{2\Delta t}\mathbf{C}_p \quad (63)$$

and

$$\mathbf{R}^k = \mathbf{F}^k - \mathbf{A}\boldsymbol{\psi}^k - \left(\mathbf{K} - \frac{2}{\Delta t^2}\mathbf{M}_p\right)\mathbf{p}^k - \left(\frac{1}{\Delta t^2}\mathbf{M}_p - \frac{1}{2\Delta t}\mathbf{C}_p\right)\mathbf{p}^{k-1} \quad (64)$$

The algebraic equations given in (62) are decoupled using standard lumping techniques to diagonalize \mathbf{M}_p and \mathbf{C}_p , e.g. using nodal (Lobatto) quadrature, row-sum technique, or the HRZ lumping scheme [23]. Using nodal lumping the effective mass $\hat{\mathbf{M}}$ is diagonal, and the system of equations (62) can be solved without factorizing a matrix; i.e., only matrix multiplications are required to obtain the right-hand-side effective load vector \mathbf{R}^k , after which the nodal pressures p_I can be updated using,

$$p_I^{k+1} = \frac{R_I^k}{\hat{m}_{II}} \quad (65)$$

where p_I^{k+1} and R_I^k denote the I th components of the vectors \mathbf{p}^{k+1} and \mathbf{R}^k , respectively, and \hat{m}_{II} is the I th diagonal element of the effective mass matrix obtained from the lumped mass and damping matrices. Furthermore, the matrix-vector products $\mathbf{A}\boldsymbol{\psi}^k$ and $\mathbf{K}_p\mathbf{p}^k$ can be evaluated at the element level by summing the contributions from each element to the effective load vector, without matrix assembly of \mathbf{A} or \mathbf{K}_p , rendering a highly efficient algorithm for large-scale wave propagation analysis.

The system of equations (47) for the auxiliary parameters $\boldsymbol{\psi}$ are not readily decoupled because of the difficulty generating an accurate diagonal matrix for \mathbf{C}_ψ using

standard lumping techniques. In this case, we compute $\boldsymbol{\psi}^{k+1}$ using the *implicit*, second-order Adams-Moulton method (trapezoidal rule), i.e.,

$$\hat{\mathbf{C}} \boldsymbol{\psi}^{k+1} = \left(\mathbf{C}_\psi - \frac{\Delta t}{2} \mathbf{K}_\psi \right) \boldsymbol{\psi}^k + \frac{\Delta t}{2} \mathbf{A}^T (\mathbf{p}^{k+1} + \mathbf{p}^k) \quad (66)$$

with

$$\hat{\mathbf{C}} = \mathbf{C}_\psi + \frac{\Delta t}{2} \mathbf{K}_\psi \quad (67)$$

Using a direct solver, and a constant time step Δt , the banded/sparse matrix $\hat{\mathbf{C}}$ is factorized only once into $\hat{\mathbf{C}} = \mathbf{L} \mathbf{D} \mathbf{L}^T$, where \mathbf{L} is a lower triangle and \mathbf{D} is a diagonal matrix. For constant wave speed c on the artificial boundary Γ , then $\mathbf{K}_\psi = \frac{c}{R} \mathbf{C}_\psi$ and the system (66) may be solved even more efficiently with the following procedure:

$$\text{Compute: } \mathbf{r}^{k+1} = \mathbf{A}^T (\mathbf{p}^{k+1} + \mathbf{p}^k) \quad (68)$$

$$\text{Solve: } \mathbf{C}_\psi \mathbf{y}^{k+1} = \mathbf{r}^{k+1} \quad (69)$$

$$\text{Update: } \boldsymbol{\psi}^{k+1} = \frac{b}{a} \boldsymbol{\psi}^k + \frac{\Delta t}{2a} \mathbf{y}^{k+1} \quad (70)$$

where $a = 1 + \gamma$, $b = 1 - \gamma$, and $\gamma = c\Delta t/2R$.

Similarly, the numerical solution \mathbf{z}_{nm}^{k+1} to the first-order system (20), and the solution q_{nm}^{k+1} to the first-order equation (42) may be computed concurrently using the implicit and unconditionally stable second-order Adams-Moulton method, i.e.,

$$\mathbf{B}_n \mathbf{z}_{nm}^{k+1} = \left(\mathbf{I} + \frac{\Delta t}{2} \mathbf{A}_n \right) \mathbf{z}_{nm}^k + \frac{\Delta t}{2} (\Phi_{nm}^{k+1} + \Phi_{nm}^k) \quad (71)$$

with

$$\mathbf{B}_n = \mathbf{I} - \frac{\Delta t}{2} \mathbf{A}_n \quad (72)$$

and then update,

$$q_{nm}^{k+1} = \frac{b}{a} q_{nm}^k + \frac{\gamma}{a} \tilde{\mathbf{c}}_n \cdot (\mathbf{z}_{nm}^{k+1} + \mathbf{z}_{nm}^k) \quad (73)$$

After the initial conditions are established, the complete mixed time-integration algorithm proceeds as follows for a fixed time step size, Δt :

1. Calculate effective loads at time t from (64),
2. Update the pressure field at time $t + \Delta t$ from (65),
3. Solve for auxiliary functions $\boldsymbol{\psi}$ at time $t + \Delta t$ from (66),
4. For each mode, solve the functions \mathbf{z}_{nm} at time $t + \Delta t$ from (71),
5. For each mode, update the functions q_{nm} at time $t + \Delta t$ from (73),
6. Update the time step, and repeat.

The key to the effectiveness of this algorithm is that the pressure update relies only on the auxiliary functions at the current time step, i.e., ψ^k and q_{nm}^k ; and the update of the auxiliary functions relies only on the most recently computed pressure at time step t_{k+1} . The result is a very natural algorithm which avoids the need for intermediate updates between equations as would be the case in a staggered-step time integration. We also note that this mixed time-integration method also provides an efficient way to implement the local B_2 boundary condition of Bayliss and Turkel [10] in symmetric form; in this case the functions z_{nm} and q_{nm} are not used, so that steps 4. and 5. may be skipped in the above algorithm.

8 Numerical Studies

In [18, 19] numerical experiments for radiation from a sphere in free-space are presented which demonstrate the accuracy of the NRBC compared to steady-state analytical solutions and standard local absorbing boundary conditions. In this work, numerical studies of fully transient solutions for a circular piston transducer mounted in an infinite rigid planar baffle are presented. Numerical results are used to assess the accuracy of the mixed explicit-implicit time integration method and the NRBC defined in (40) - (42) for a half-space problem defined by a rigid baffle. Both sinusoidal and Gaussian pulse surface velocities are used to drive the transient solutions. A circular transducer radiating into an acoustic fluid is considered since this case has been widely studied and is important to many researchers.

8.1 Circular Piston In A Rigid Planar Baffle

We first consider a circular transducer of radius a , oscillating perpendicular to the plane of a rigid infinite baffle. The sound pressure field is determined by the wave equation and boundary conditions,

$$\frac{\partial p}{\partial z} = \begin{cases} -\rho_o \dot{v}(t) H(t), & \text{on piston P} = \{0 \leq r \leq a, \theta = \pi/2\} \\ 0, & \text{on baffle B} = \{r > a, \theta = \pi/2\} \end{cases} \quad (74)$$

where $H(t)$ is the Heaviside (unit step) function. Here, z is the coordinate normal (perpendicular) to the piston and baffle, $v(t)$ is the normal velocity of the piston, and a superimposed dot denotes a time derivative.

The sound field $p(r, \theta, t)$ is rotationally symmetric about the z -axis normal to the center of the piston and independent of φ . Since the problem is axisymmetric, it is convenient to introduce cylindrical coordinates (ρ, z) , where $\rho = r \sin \theta$ is the polar radius.

8.1.1 SINUSOIDAL INPUT

We first assume that the piston velocity in Eq. (74) is sinusoidal for $t \geq 0$, with

$$v(t) = 1 - \cos \omega t \quad (75)$$

resulting in a pressure gradient for $t \geq 0$,

$$\frac{\partial p}{\partial z} = -\rho_o \omega \sin \omega t \quad \text{on piston P} \quad (76)$$

where ω is a radian frequency.

The steady-state response along the z -axis for the sinusoidal input (75), is available in a closed-form analytical solution given in [24]:

$$p(0, z, t) = \text{Imag} \left\{ i \rho_o c e^{i\omega t} \left[e^{-ikz} - e^{-ik\sqrt{z^2+a^2}} \right] \right\} \quad (77)$$

where c is the speed of sound, and $k = \omega/c$ is the wave number. A study of the pressure amplitude on the axis of this piston reveals that the axial response exhibits strong interference effects, fluctuating between 0 and $2\rho_o c$. These zero pressure amplitudes occur at points z_m satisfying the condition,

$$\frac{z_m}{a} = \frac{1}{m} \frac{a}{\lambda} - \frac{m}{4} \frac{\lambda}{a} \quad (78)$$

where $\lambda = 2\pi/k$, and $m = \text{even}$.

Immediately after the circular piston (transducer) is switched on, the acoustic field will undergo a transient solution that is quite different from the steady-state condition; the radiation impedance consists of high frequency components only, and then rapidly approaches the steady state value. Since the rigid vibrating piston can be considered to be a distribution of point sources, the sound field occupies a region in space which is obtained by locating spheres of radius ct from each point on the piston. Thus the pressure on the piston itself is transient for the first $2a/c$ seconds, which is the time required for a signal to propagate from one edge of the piston across to the opposite edge. The pressure on the piston after the first $2a/c$ seconds is the same as in the steady-state.

The transient sound field is available in a closed-form expression that can be integrated numerically [25]. The velocity potential field ϕ is represented as the time convolution of the normal velocity of the piston and a radiation impulse response:

$$\phi(\rho, z, t) = v(t) * h(\rho, z, t) \quad (79)$$

where the asterisk is used to denote the convolution operation, h is the velocity potential impulse response, t is the time, and a is the radius of the circular piston. The acoustic velocity in the medium is the negative gradient of the velocity potential ϕ , given by $\mathbf{v} = -\nabla\phi$. The pressure may then be obtained from the velocity potential using the relationship $p = \rho_o \dot{\phi}$.

The impulse response function $h(\rho, z, t)$ is the time-dependent velocity potential field resulting from a Dirac impulsive z -velocity of the piston [25]:

$$h(\rho, z, t) = \begin{cases} c, & \rho < a, \quad z < ct < R_1, \\ \frac{c}{\pi} \cos^{-1} \left(\frac{c^2 t^2 - z^2 + \rho^2 - a^2}{2\rho\sqrt{c^2 t^2 - z^2}} \right), & R_1 < ct < R_2, \\ 0, & \text{elsewhere,} \end{cases} \quad (80)$$

where $R_1 = \sqrt{z^2 + (a - \rho)^2}$, and $R_2 = \sqrt{z^2 + (a + \rho)^2}$, are the shortest and longest distances, respectively, from the observation point to the circumference of the piston.

For observation points on the z -axis, $R_1 = R_2 = \sqrt{z^2 + a^2}$, so that h is a delayed rectangular pulse, and the time convolution given in (79) may be evaluated in closed-form:

$$p(0, z, t) = \rho_o c \left\{ v \left(t - \frac{z}{c} \right) H \left(t - \frac{z}{c} \right) - v \left(t - \frac{\sqrt{z^2 + a^2}}{c} \right) H \left(t - \frac{\sqrt{z^2 + a^2}}{c} \right) \right\} \quad (81)$$

where $H(t)$ is the Heaviside function. The pressure on the z -axis is thus seen to consist of two signals of opposite strength equal to the characteristic impedance $\rho_o c$.

Since the problem is axisymmetric, it is sufficient to compute the finite element solution in the two-dimensional domain Ω defined by the (r, θ) plane for $0 \leq r \leq R$, and $0 \leq \theta \leq \pi/2$. The pressure field is approximated with 4-node bilinear axisymmetric acoustic elements with a non-reflecting boundary applied to a quarter-circle truncation boundary $\Gamma := \{r = R, 0 < \theta \leq \pi/2\}$.

For the finite element solution, the truncation boundary Γ is positioned close to the radius of the piston at $R/a = 1.25$, resulting in a relatively small computational domain. The piston radius and wave speed are normalized such that $a = 1$ and $c = 1$. The calculation is then driven with a normalized frequency $\omega a/c = 4\pi$ on a mesh with 150 evenly spaced elements along the z -axis from $0 \leq z \leq 1.25$, and 90 evenly spaced elements from $0 < \theta \leq \pi/2$. For this frequency and piston radius, the zero amplitude points along the z -axis occur at $z_2 = 0.75$, and at the origin $z_4 = 0.0$.

A time-harmonic solution is obtained by starting from rest with initial data p_0 and \dot{p}_0 equal to zero and driving the solution to steady-state with a time step $\Delta t = 0.003$ sec. The mesh and time step size are small relative to the wavelength $\lambda = 0.5$, so that numerical error is due primarily to the the radiation boundary condition on Γ .

Fig. 2 shows time-dependent solutions at several observation points along the z -axis obtained using the local B_1 and B_2 operators, and the nonreflecting boundary condition NR2(20), compared to the analytical solution. Fig. 3 shows time-histories at several locations on the truncation boundary Γ . The numerical solution obtained using NR2(20) can barely be distinguished from the analytical solution at all locations, including the interference point $z = 0.75$, where the steady-state amplitude is zero. The solution using B_2 exhibits relatively accurate solutions for points off-axis, however significant amplitude errors occur for points on the z -axis. The B_1 operator yields both large amplitude and phase errors, at all observation points except the piston origin $z = 0$, where all the operators accurately represent the solution, even during the zero steady-state amplitude phase. This interesting result is expected since at this location and for a piston of infinite radius it can be shown that the pressure and normal velocity at $z = 0$ are related by the simple plane-wave relationship $p = \rho_o c v$, which is accurately represented by all of the boundary conditions considered.

The instantaneous error measured in L_2 norm on the z -axis is defined as,

$$E(t) = \left\{ \int_0^R [p^h(z, t) - p(z, t)]^2 dz \right\}^{1/2} \quad (82)$$

where p^h is the approximate finite element solution and p is the exact steady-state

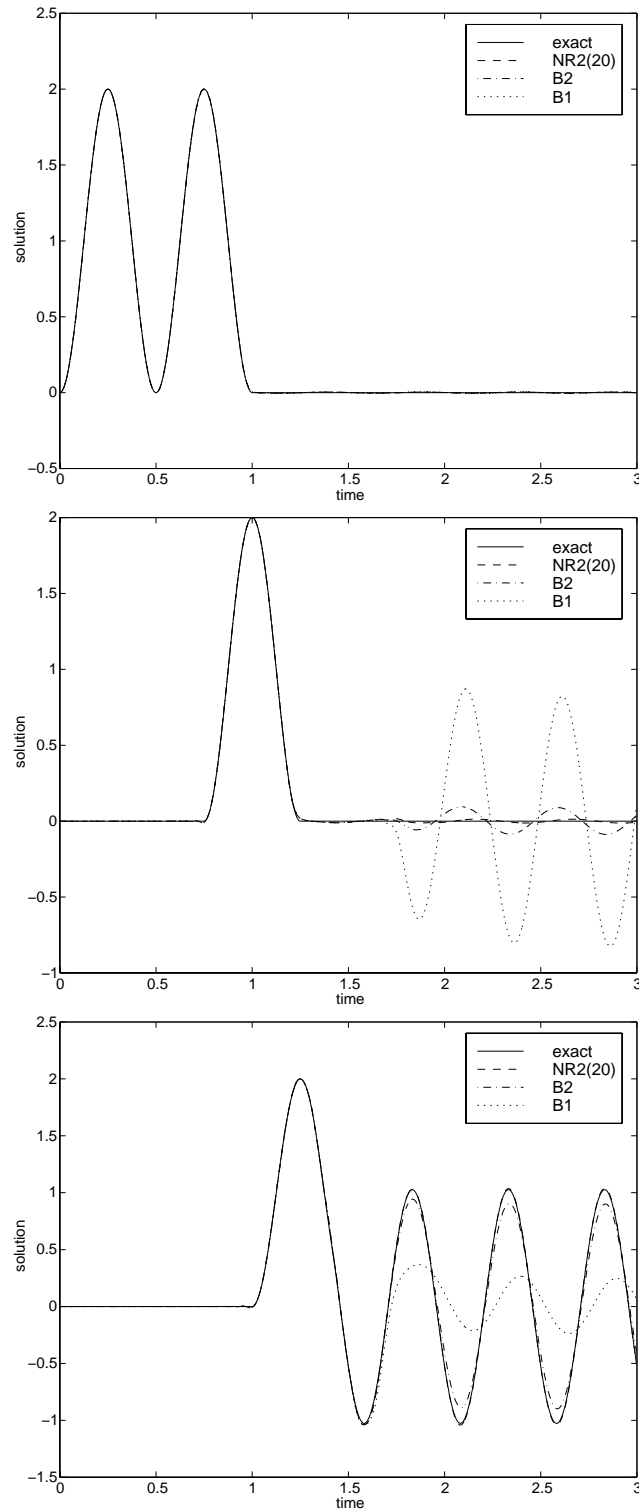


Fig. 2: Sinusoidal Input. Time-histories at on-axis observation points: (a) $z = 0.0$; (b) $z = 0.75$; (c) $z = 1.0$.

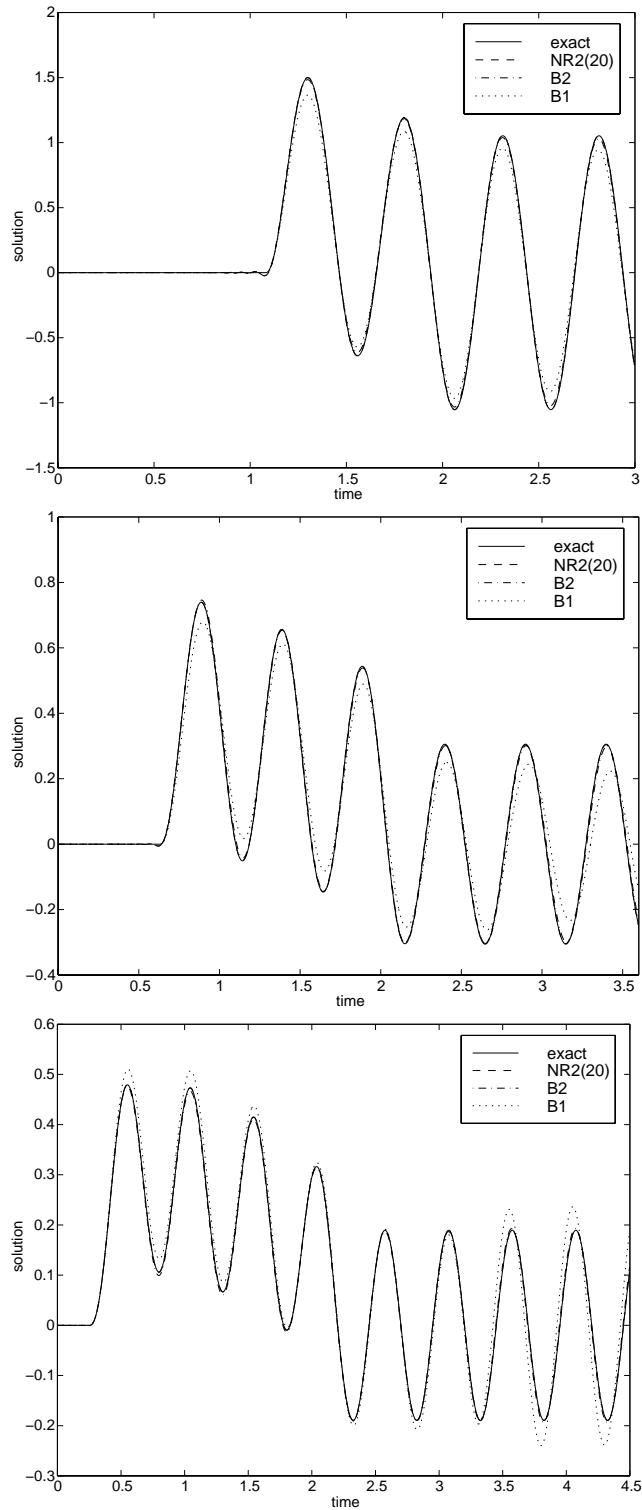


Fig. 3: Sinusoidal Input. Time-histories at off-axis observation points on truncation boundary at $R = 1.25$, and $\theta = 30, 60, 90$ degrees.

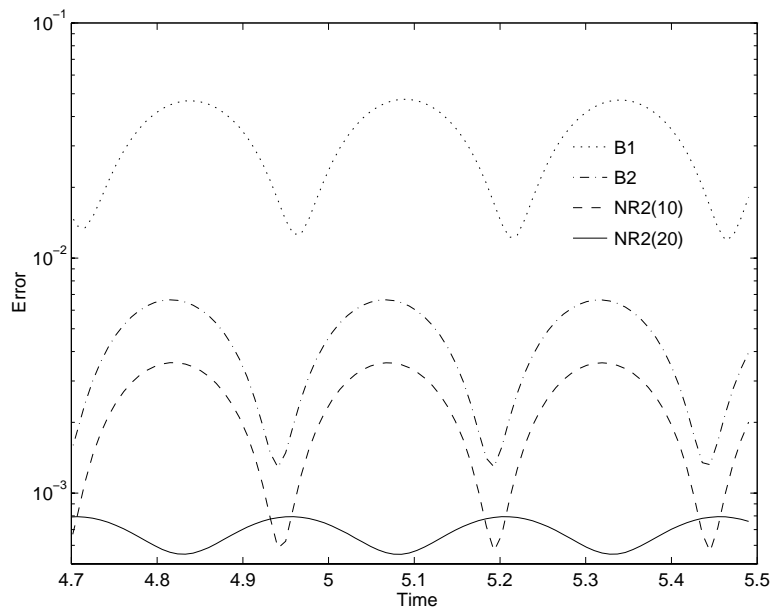


Fig. 4: Instantaneous error $E(t)$ along the z -axis and at steady-state due to a sinusoidal radiating circular piston with normalized frequency $\omega a/c = 4\pi$ and truncation boundary radius $R/a = 1.25$. Results compared for local operators B_1 , B_2 , and boundary condition $\text{NR2}(N)$, with series truncation $N = 10$ and $N = 20$.

solution, and $R = 1.25$. The magnitude of the absolute error $E(t)$ can be scaled by any constant, and will only serve as a means to compare the relative accuracy of the different boundary conditions. Fig. 4 shows the instantaneous error on the piston axis and over the steady-state time interval $4.7 < t < 5.5$. The results illustrate the reduction in error obtained from $\text{NR2}(N)$ by increasing the number of terms in the truncated series from $N = 10$ to $N = 20$. The accuracy of the $\text{NR2}(20)$ solution is significantly improved over the local B_2 operator. We also observe that the error using the nonreflecting boundary condition $\text{NR2}(20)$ reduced by an order of magnitude compared to the local B_1 boundary condition.

8.1.2 GAUSSIAN PULSE

We next study the response due to a transient pulse which excites a range of frequencies. The piston velocity is assumed to be the Gaussian pulse,

$$v(t) = e^{-0.5f_o^2(t-t_o)^2} H(t) \quad (83)$$

where $t_o = 0.5$ s, and $f_o = 8$. The frequency spectrum of this wavelet is,

$$v(\omega) = \frac{\sqrt{2\pi}}{f_o} e^{-0.5\omega^2/f_o^2} \quad (84)$$

Fig. 5 shows the pulse, and its amplitude spectrum.

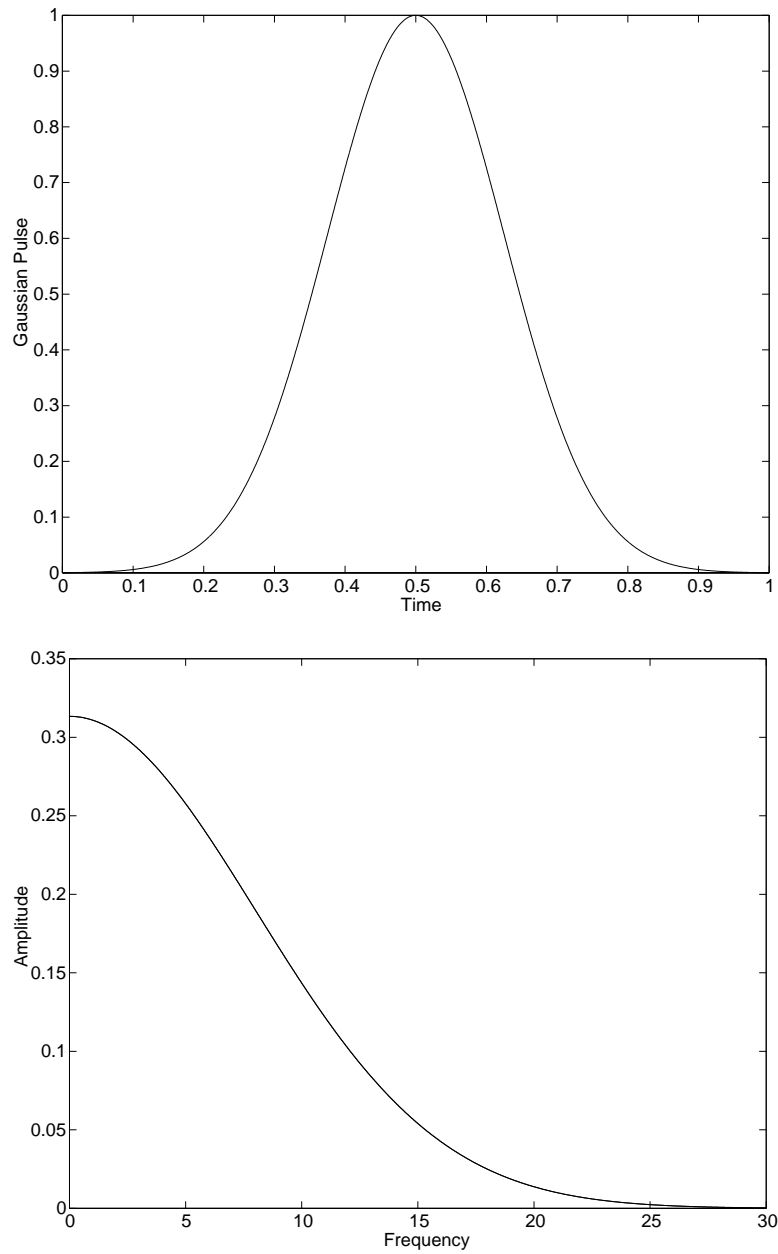


Fig. 5: Gaussian pulse and its Fourier transform: (a) Gaussian pulse versus time; (b) The amplitude spectrum versus frequency ω .

For this input, the pressure on the z -axis consists of two Gaussian pulses of opposite amplitude. The time delay of the initial pulse corresponds to the propagation time from the center of the piston to the spatial point, and the time delay of the second pulse corresponds to the propagation time from the edge of the piston to the spatial point.

The computations are performed with the element size, and time-step unchanged from the previous study. Fig. 6 and Fig. 7 show contours of the pressure field solution using NR2(20) at several time steps. Fig. 8 shows transient solutions at several observation points on the z -axis. Fig. 9 shows time-histories at different locations on the truncation boundary Γ . Comparisons are made between the analytical solution and finite element solutions using the local operators B_1 and B_2 , and the non-reflecting condition NR2(N), with series truncation $N = 20$. The solution obtained using NR2(20) can barely be distinguished from the analytical solution at all observation points. The early time response is accurately represented on the z -axis using any of the boundary conditions studied. However, the numerical solution for B_1 exhibits large errors during the second pulse; both overshooting and undershooting the exact solution. The solution using B_2 shows significant error at the trailing end of the second pulse. On the truncation boundary, at angles off the piston axis, the local boundary operators exhibit spurious reflections during both the initial and secondary pulses. It is observed that both the local operators and nonreflecting condition NR2(N), accurately represent the solution at the center of the piston $z = 0$, for all time.

9 Conclusions

An extension of the exact nonreflecting boundary condition (NRBC) first derived by Grote and Keller [17] for the free-space problem, is formulated on a hemisphere for the time-dependent wave equation in a half-space defined by a planar baffle. Since the problem is symmetric about the infinite planar surface, we show that it is sufficient to restrict the spherical harmonic expansion which defines the NRBC to indices $n + m$ even, and scale the radial harmonics by a factor of 2, in order to satisfy the rigid baffle condition. In this case, we position the baffle normal (perpendicular) to a z -axis in spherical coordinates. Since the symmetry condition is imposed with the Legendre function expansion in θ , the Fourier expansion in the circumferential angle φ may be used to efficiently model axisymmetric problems in two-dimensions. Alternatively, the NRBC for the half-space problem may be formulated based on a z -axis aligned parallel to the planar baffle. In this case the Fourier expansion in the circumferential angle is restricted to even functions in order to satisfy the rigid baffle symmetry condition. While this alternative form of the NRBC has the same number of operation counts and memory requirements in general three-dimensional problems, it cannot be used for the axisymmetric problem since the Fourier harmonics are restricted by the baffle condition. Symmetry conditions for the planar baffle may also be applied to recently developed asymptotic radiation boundary conditions given in [26] which have improved efficiency over the exact condition.

For the symmetric form of the modified NRBC we developed a new mixed explicit-implicit time integration method which retains the efficiency of explicit time dis-

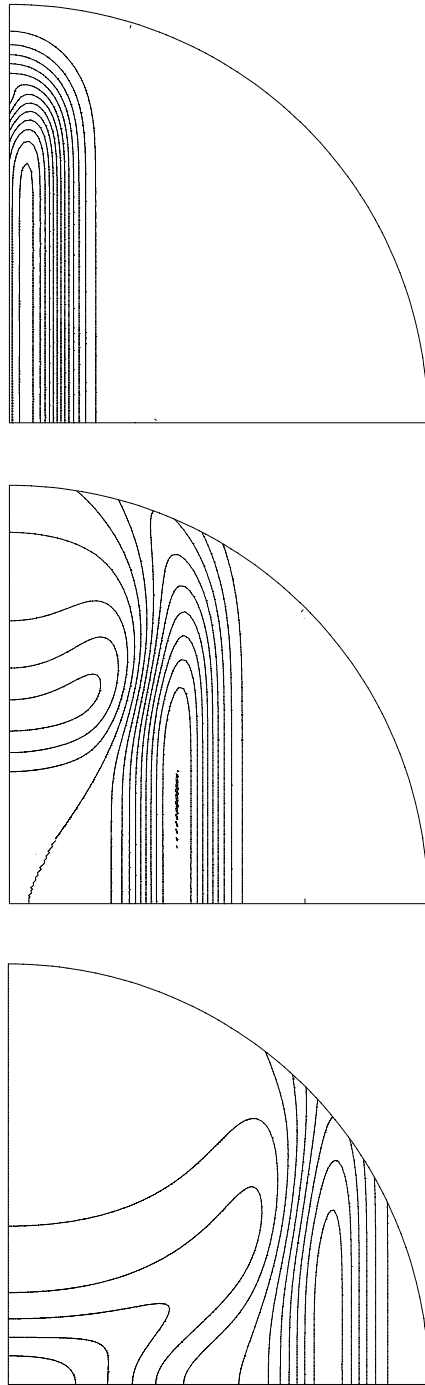


Fig. 6: Solution contours of pressure field using NR2(20) for transient radiation from a circular piston in infinite planar baffle with Gaussian normal velocity at time (a) $t = 0.45$; (b) $t = 0.9$; (c) $t = 1.35$.

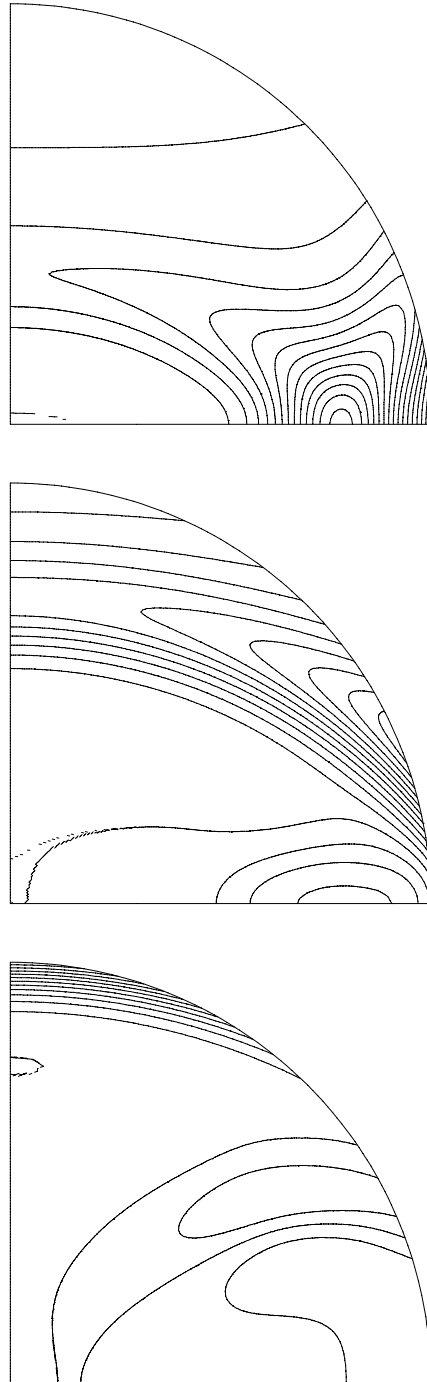


Fig. 7: Solution contours of pressure field using NR2(20) for transient radiation from a circular piston in infinite planar baffle with Gaussian normal velocity at time (a) $t = 1.8$; (b) $t = 2.25$; (c) $t = 2.7$.

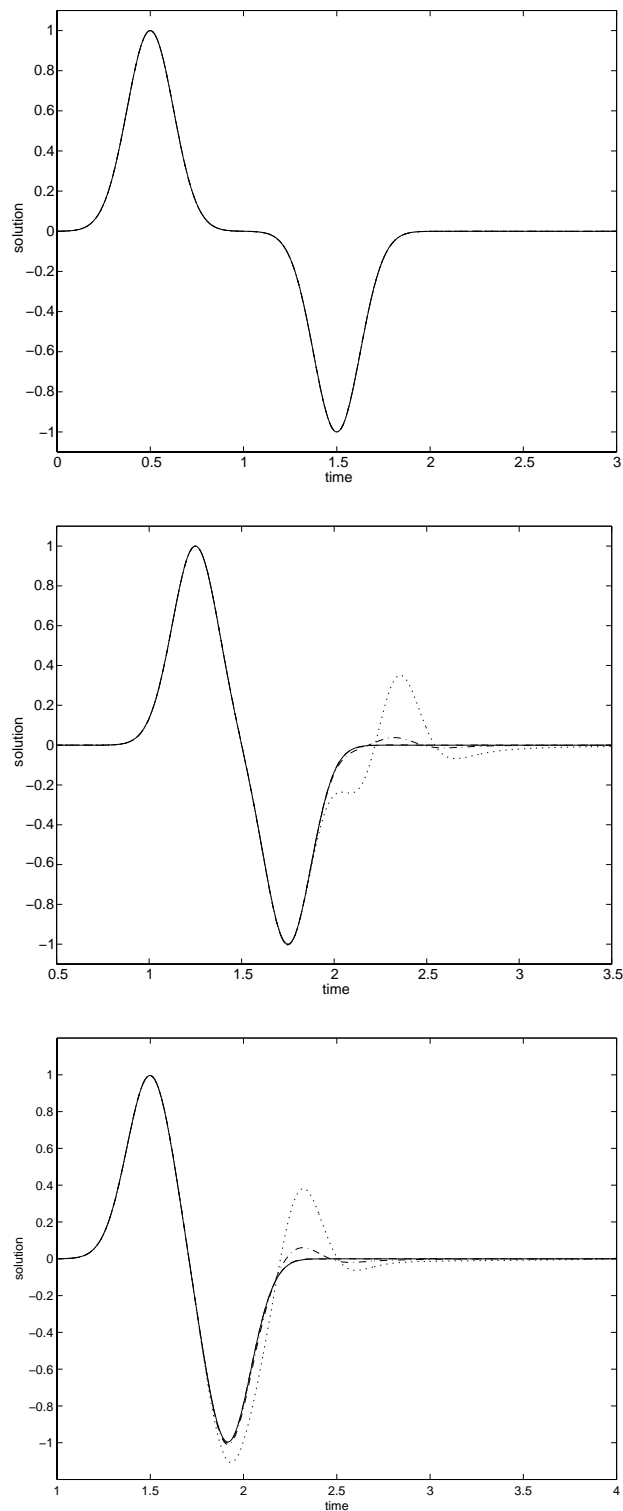


Fig. 8: Gaussian Pulse. Time-histories at on-axis observation points: (a) $z = 0.0$; (b) $z = 0.75$; (c) $z = 1.125$. Solid lines denote analytic solution; Dashed lines denote NR2(20); Dash-dotted lines denote B_2 ; Dotted lines denote B_1 .

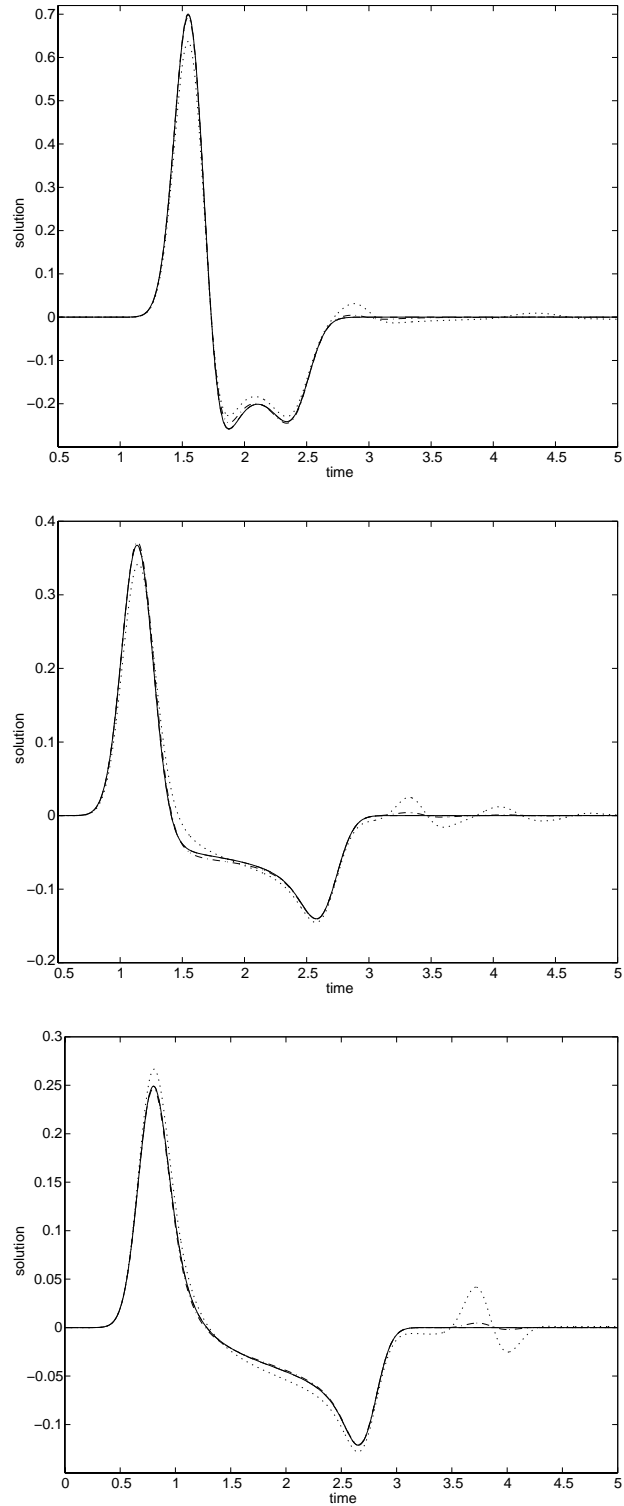


Fig. 9: Gaussian Pulse. Time-histories at off-axis observation points on truncation boundary at $R = 1.25$: (a) $\theta = 30$; (b) $\theta = 60$; (c) $\theta = 90$ degrees. Solid lines denote analytic solution; Dashed lines denote NR2(20); Dash-dotted lines denote B_2 ; Dotted lines denote B_1 .

cretization for the finite element matrix equations, without the need for diagonal matrices in the auxiliary equations on the artificial truncation boundary. Here, the interior finite element equations are integrated explicitly in time while the auxiliary equations on Γ are integrated implicitly in time. By treating the auxiliary equations implicitly, a very natural algorithm results which avoids the need to update either the pressure solutions or the auxiliary functions at intermediate time steps and which retains the second-order accuracy of the underlying methods. The key to the effectiveness of the scheme is that the pressure update relies only on the auxiliary functions at the current time step, and the update of the auxiliary functions relies only on the most recently computed pressure at time step t_{k+1} . The result is a very natural and highly efficient algorithm for large-scale wave propagation analysis which allows the pressure field to be updated without assembling or factoring the interior finite element matrices. This mixed time-integration method also provides an efficient way to implement the local B_2 boundary condition of Bayliss and Turkel.

Numerical examples of fully transient radiation from a circular piston transducer mounted in an infinite rigid planar baffle demonstrate the improved accuracy of the NRBC and the new mixed explicit-implicit time integration method compared to the first- and second-order local boundary conditions of Bayliss and Turkel. For a sinusoidal normal velocity input, the transient solution obtained using NR2(20) can barely be distinguished from the analytical solution at all points in the computational domain, including the difficult interference point on the piston axis where the steady-state amplitude is zero. The solution using the local second-order operator exhibits relatively accurate solutions for points off-axis, however significant amplitude errors occur for the difficult points on the piston axis. The local first-order operator yields both large amplitude and phase errors, at all observation points except the piston origin. Similar results are found for a Gaussian pulse input. The accuracy of the local operators may be improved by moving the artificial truncation boundary further away from the source of radiation at the expense of a larger computational domain with increased work. In other numerical studies [17], it is shown that the extra work in employing the local conditions with a large mesh is several times larger than the work required to compute the spherical harmonics in the exact NRBC on a smaller mesh. An important area of future work is to determine the benefit of increased accuracy using the modified NRBC with the extra expense in computing the auxiliary functions ψ at each node on the artificial boundary.

Acknowledgements

Support for this work was provided by the National Science Foundation under Grant CMS-9702082 in conjunction with a Presidential Early Career Award for Scientists and Engineers (PECASE), and is gratefully acknowledged. We would also like to thank the anonymous reviews for helping to clarify the alternative methods for satisfying the rigid baffle condition.

References

- [1] R. Bossut, and J-N. Decarpigny, 'Finite element modeling of radiating structures using dipolar damping elements', *J. Acoust. Soc. Am.* **86** (4), pp. 1234 – 1244 (1989).
- [2] F. Coulouvrat, 'Continuous field radiated by a geometrically focused transducer: Numerical investigation and comparison with an approximate model', *J. Acoust. Soc. Am.* **94** (3), pp. 1663 – 1675 (1993).
- [3] K.J. Hays-Stang and B.D. Cook, 'Investigation of ultrasonic pulses with an optical probe', *J. Acoust. Soc. Am.* **97** (4), pp. 2210 – 2217 (1995).
- [4] G. Wojcik, J. Mould, F. Lizzi, N. Abboud, M. Ostromogilsky, and D. Vaughan, 'Nonlinear modeling of therapeutic ultrasound', *IEEE Ultrasonics Symposium Proceedings*, pp. 1–6 (1995).
- [5] W. Friedrich, P. Krammer, R. Lerch, 'Finite element modeling of acoustic radiation from piezoelectric phased array antennas', *Proceedings IEEE Ultrasonics Symposium*, **35**, pp. 763–767 (1990).
- [6] S. Tsynkov, 'Numerical solution of problems on unbounded domains. A review', *Appl. Num. Math.* **27**, 465-532, 1998.
- [7] J. B. Keller and D. Givoli, 'Exact non-reflecting boundary conditions', *J. Comp. Phys.*, 82 (1989), pp. 172–192.
- [8] L.L. Thompson, R. Huan and C. Ianculescu, 'Finite Element Formulation Of Exact Dirichlet-to-Neumann Radiation Conditions on Elliptic and Spheroidal Boundaries', *Proceedings of the ASME Noise Control and Acoustics Division – 1999*, 1999 ASME International Mechanical Engineering Congress and Exposition, Nashville, TN. Symposium on Computational Acoustics, NCA-Vol. 26, pp. 497 - 509.
- [9] D. Burnett, 'A 3-D acoustic infinite element based on a generalized multipole expansion', *J. Acoust. Soc. Am.*, **96**, (1994), pp. 2798-2816.
- [10] A. Bayliss and E. Turkel, 'Radiation boundary conditions for wave-like equations', *Commun. Pure Appl. Math.*, **33**, pp. 707–725 (1980).
- [11] P. M. Pinsky and N. N. Abboud, 'Finite element solution of the transient exterior structural acoustics problem based on the use of radially asymptotic boundary operators', *Comput. Methods Appl. Mech. Engrg.* **85**, pp. 311–348 (1991).
- [12] P. M. Pinsky, L. L. Thompson, and N. N. Abboud, 'Local high-order radiation boundary conditions for the two-dimensional time-dependent structural acoustics problem', *J. Acoust. Soc. Am.* **91** (3), pp. 1320–1335 (1992).

- [13] L. L. Thompson and P. M. Pinsky, ‘A space-time finite element method for structural acoustics in infinite domains, Part 2: Exact time-dependent non-reflecting boundary conditions’, *Comput. Methods Appl. Mech. Engrg.* **132**, pp. 229-258 (1996).
- [14] Q.H. Liu, and J. Tao, ‘The perfectly matched layer (PML) for acoustic waves in absorptive media’, *J. Acoust. Soc. Am.*, **102**, 2072-2082, (1997).
- [15] X. Yuan, D. Borup, J.W. Wiskin, M. Berggren, R. Eidsens, and S.A. Johnson, ‘Formulation and validation of Berenger’s PML absorbing boundary for the FDTD simulation of acoustic scattering’, *IEEE Trans. Ultrason., Ferroelect., Freq. Contr.*, **44**, 816-822 (1997).
- [16] M. J. Grote and J. B. Keller, ‘Exact non-reflecting boundary conditions for the time dependent wave equation’, *SIAM J. of Appl. Math.*, **55**, pp. 280–297 (1995).
- [17] M. J. Grote and J. B. Keller, ‘Nonreflecting boundary conditions for time dependent scattering’, *J. of Comput. Phys.*, **127**, pp. 52–65 (1996).
- [18] L. L. Thompson and R. Huan, ‘Implementation of Exact Non-Reflecting Boundary Conditions in the Finite Element Method for the Time-Dependent Wave Equation’, *Computer Methods in Applied Mechanics and Engineering*, (in press).
- [19] L. L. Thompson and R. Huan, ‘Finite Element Formulation of Exact Non-Reflecting Boundary Conditions for the Time-Dependent Wave Equation’, *International Journal for Numerical Methods in Engineering*, **45**, pp. 1607-1630, (1999).
- [20] L.L. Thompson, and R. Huan, ‘Computation of far field solutions based on exact nonreflecting boundary conditions for the time-dependent wave equation’, *Computer Methods in Applied Mechanics and Engineering*, **190**, pp. 1551-1577, (2000).
- [21] E. W. Hobson, *Spherical and Ellipsoidal Harmonics*, (Cambridge University Press, 1955).
- [22] H. Lamb, *Hydrodynamics*, Fourth Edition, (Cambridge University Press, 1916), p. 517, eq.4.
- [23] R. D. Cook, D. S. Malkus, M. E. Plesha, *Concepts and applications of finite element analysis*, Third Edition, (John Wiley & Sons, New York, 1989).
- [24] P. M. Morse and H. Feshbach, *Methods of Theoretical Physics*, Vol II, (McGraw-Hill, 1953).
- [25] P. R. Stepanishen, ‘Transient Radiation from Pistons in an Infinite Planar Baffle’, *J. Acoust. Soc. Am.* **49** (5), pp. 1629 – 1638 (1971).
- [26] R. Huan and L. L. Thompson, ‘Accurate Radiation Boundary Conditions for the Time-Dependent Wave Equation on Unbounded Domains’, *International Journal for Numerical Methods in Engineering*, **47**, pp. 1569-1603 (2000).